Concerning the Feasibility of a Real-Time SAR Digital Processor for VOIR Low Resolution Imaging Modes

T. K. Truong and R. G. Lipes
Communications Systems Research Section

In this article, the feasibility of real-time digital processing of synthetic aperture radar data for Venus Orbiting Imaging Radar low resolution modes is investigated. First, it is shown that range migration is not a problem for these modes. Then, under the assumption of no range migration, fast Fourier transform implementations for accomplishing both range and azimuth correlation in real-time are shown to be feasible with current technology. Treatment of other important aspects of real-time processing such as automatic focusing and Doppler centroid location is deferred to subsequent articles.

I. Introduction

An efficient synthetic aperture radar (SAR) processing algorithm such as the one proposed in this article could provide the basis for a real-time SAR correlator implementation in the Deep Space Network (DSN). A real-time SAR correlator located in a DSN station would reduce the high-rate SAR raw data, expected from the proposed Venus Orbiting Imaging Radar (VOIR) mission of the mid 1980s, directly into lower rate image data. This could introduce savings in both time and costs by potentially eliminating the transport of high density tapes of raw SAR data from DSN stations to JPL for processing. Furthermore, it would provide a quick-look capability for verifying that SAR sensor and data communications are operating as expected.

One problem in investigating the feasibility of real-time SAR processing for the VOIR mission arises from changes in mission requirements as different approaches are explored and funding baselines are altered. To avoid tracking these changes, an interim set of requirements (Ref. 1) was chosen as a basis for the feasibility study, with the realization that a final set exhibiting large departures from this set could alter the conclusions. The approach to the feasibility study was to develop a conceptual design that could be implemented with proven special purpose hardware. Furthermore, the initial design discussed in this article was not required to accommodate SAR data with significant range migration. Subsequent studies will address processing techniques for such data.

In Section II, the extent of range migration is determined for the various options in Ref. 1. Only the low-resolution mode is essentially free of range migration. For this mode, a design based on a fast Fourier transform (FFT) implementation is presented. In Sections III and IV, the feasibility of real-time correlation in range and azimuth respectively is demonstrated.

II. Computation of Range Migration of VOIR-SAR Processor

A set of VOIR system characteristics given in Ref. 1 is given in Table 1. From Table 1, one observes that two sets of parameters of low resolution and high resolution at incidence angles $\theta = 25$ and $\theta = 52$ are given. To compute the range migration for these two imaging modes, let

f: carrier frequency

L_a: azimuth length of reference filter per look

L: total azimuth length of reference filter

λ: wavelength

R: slant range

ΔZ: azimuth resolution

ΔR: range resolution

N: number of looks

Δx: pixel spacing in the final imagery

τ_a: integration time per look

ΔR_c: range curvature

ΔR_w: range walk

ΔR_m: range migration

v: the nominal spacecraft speed

B: bandwidth of the pulse

f_s: sampling frequency

f_d: doppler center frequency

H: altitude

θ: incident angle

c: speed of light

PRF: pulse repetition frequency

It was shown (Ref. 2) that the azimuth length of the reference filter per look is

$$L_a = \frac{\lambda R}{2\Delta Z} \tag{1a}$$

where R is defined by

$$R = \frac{H}{\cos\theta} \tag{1b}$$

Then the actual azimuth length of the reference filter is

$$L = NL_a = N\frac{\lambda R}{2\Delta Z} \tag{2}$$

It was also shown (Refs. 3 and 4) that the range curvature and the range walk of the reference filter are

$$\Delta R_c = \frac{L^2}{8R} \tag{3}$$

and

$$\Delta R_w = \frac{\lambda}{2}(f_d N \tau_a) \tag{4a}$$

where τ_a is given by

$$\tau_a = \frac{L_a}{v} \tag{4b}$$

and the range migration is given by

$$\Delta R_m = \Delta R_c + \Delta R_w \tag{5}$$

The sampling frequency is defined by

$$f_s \cong 1.2\,B > B$$

The pixel spacing of the final imagery is given by

$$\Delta x = \frac{c}{2f_s} \tag{6}$$

Note that if $\Delta R_m \leqslant \Delta x$, then range migration is not important. Otherwise, range migration must be treated.

From the parameters given in Table 1 and the assumption of 1 KHz as a representative doppler center frequency, one can compute the range migration of the high-resolution and the low-resolution imaging modes as follows:

Case 1: High-resolution imaging mode from Eq. (6),

$$\Delta x = \frac{c}{2f_s} = \frac{2.998 \times 10^8}{2 \times 1.2 \times 4.75 \times 10^6} = 26.3 \text{ m}$$

$$\lambda = \frac{c}{f} = \frac{2.998 \times 10^8}{12.75 \times 10^8} = 0.235 \text{ m}$$

(a) For $\theta = 25°$,

$$R = \frac{H}{\cos\theta} = \frac{300\text{ km}}{\cos 25°} = 331.13\text{ km}$$

$$L_a = \frac{\lambda R}{2\Delta Z} = \frac{0.235 \times 331.13 \times 10^3}{2 \times 50} = 778\text{ m}$$

$$\Delta R_c = \frac{1}{8}\frac{(8L_a)^2}{R} = \frac{8 \times (778)^2}{331.13 \times 10^3} = 14.6\text{ m}$$

$$\tau_a = \frac{L_a}{v} = \frac{778\text{ m}}{6600\text{ m/s}} = 0.12\text{ sec}$$

$$\Delta R_w = \frac{\lambda}{2}(f_d \times 8\tau_a) = \frac{0.235}{2}(1000 \times 8 \times 0.12) = 121\text{ m}$$

$$\Delta R_m = \Delta R_c + \Delta R_w = 14.6 + 121\text{ m} = 136\text{ m}$$

Note that for this case,

$$\Delta R_c = 14.6\text{ m} < \Delta x = 26.3\text{ m}$$

$$\Delta R_m = 136\text{ m} > \Delta x = 26.3\text{ m} \qquad (7)$$

(b) For $\theta = 52°$,

$\Delta R_c = 21.5$ m, $\Delta R_w = 180$ m, and

$$\Delta R_m = \Delta R_c + \Delta R_w = 21.5 + 180 = 201.5\text{ m}$$

Note that

$$\Delta R_c = 21.5\text{ m} < \Delta x = 26.3\text{ m}$$

$$\Delta R_m = 201.5\text{ m} > \Delta x = 26.3\text{ m} \qquad (8)$$

Case 2: Low-resolution imaging mode. From Eq. (6), one obtains

$$\Delta x = 156\text{ m} \quad \text{and} \quad \lambda = 0.235\text{ m}$$

(a) For $\theta = 25°$,

$\Delta R_c = 3.6$ m, $\Delta R_w = 53.58$ m, and

$\Delta R_m = 57.18$ m

Note that

$$\Delta R_c = 3.6\text{ m} < \Delta x = 156\text{ m}$$

$$\Delta R_m = 57.18\text{ m} < \Delta x = 156\text{ m} \qquad (9)$$

(b) For $\theta = 52$,

$\Delta R_c = 2.8$ m, $\Delta R_w = 81.78$ m, and

$\Delta R_m = 84.58$ m

Note that

$$\Delta R_c = 2.8\text{ m} < \Delta x = 156\text{ m}$$

$$\Delta R_m = 84.58\text{ m} < \Delta x = 156\text{ m} \qquad (10)$$

From the above results, it follows that the range curvature of both high- and low-resolution imaging modes with $\theta = 25°$ and $\theta = 52°$ is less than the pixel spacing, and will be neglected. From Eqs. (9) and (10), the range migration is less than the pixel spacing for the low-resolution imaging mode. Thus, FFT techniques can be used to compute the real-time VOIR-SAR range correlation and azimuth correlation. From Eqs. (7) and (8), the range migration is greater than the pixel spacing for the high-resolution imaging mode.

III. Implementation of the Range Correlator

In order to compute the range correlation (Fig. 1), one needs to compute the number m of range points and the number ℓ of the pulse width points, for the low-resolution imaging mode. The number of range points is given by

$$m = f_s \frac{2x}{c} \sin\theta \qquad (11)$$

where f_s is a sampling frequency, x is a swath width, c is the speed of light. The number of pulse width or range filter points is given by

$$\ell = f_s \times \text{pulse length} \qquad (12)$$

Note that the values of the parameters in Eqs. (11) and (12) are given in Table 1.

For low-resolution imaging mode, we consider two cases:

Case 1: $\theta = 25°$, from (11) and (12),

$$m \cong 108\text{ points}; \qquad \ell \cong 26\text{ points} \qquad (13)$$

Case 2: $\theta = 52^\circ$, from (11) and (12),

$$m \cong 252; \qquad \ell \cong 26 \text{ points} \tag{14}$$

To use the FFT (Ref. 5) for implementing the range correlator, let

a: input rate, samples/sec

$R1, R2$: m-point buffers, points

n: length of the FFT, points

$T1$: computation time to load m range data points into a buffer, sec

$T2$: computation time of the range correlator using the n-point FFT, sec

r: number of points of range after range correlation (each point is 4 bits)

A detailed design of a range correlator for the low-resolution imaging mode is given in Fig. 2. Its operation is accomplished as follows:

First, load m points of range data into $R1$ buffer. The data are then passed to the range correlator for processing while buffer $R2$ is being filled. Once the processing is completed in the range correlator, only $r = n - \ell + 1$ values become output. The process is repeated for data from buffer $R2$. Note that if $T2 < T1$, then the FFT can be used to compute one-dimensional range correlation. The time $T1$ in Fig. 2 is given by

$$T1 = m/a \text{ sec} \tag{15}$$

In order to use two FFTs and the pipeline technique to correlate the ℓ-point range filter with m-point input data, one needs to choose n such that $n \geqslant m$, where n is a power of 2. If the time for computing the n-point FFT is τ_n, then $T2$ is given by

$$T2 = \tau_n \text{ sec} \tag{16}$$

Case 1: For $\theta = 25^\circ$, from Eq. (13), $m = 108$ and $\ell = 26$. Thus if one chooses $n = 128 > 108$, then the input rate for $\theta = 25^\circ$ is given by

$$a = 108 \times PRF$$

$$= 108 \times 2180 \cong 236965 \text{ samples/sec}$$

where $PRF = 2180$ Hz is given in Table 1.

From Eq. (15) it follows that

$$T1 = \frac{1}{236965} \times 108 = 4.56 \times 10^{-4} \text{ sec} \tag{17}$$

Since the JPL RFI Processor takes 6.4 μs and 12.8 μs to compute a 128-point and 256-point FFT respectively, by Eq. (17)

$$T2 = 6.4 \ \mu\text{sec} \tag{18}$$

From Eqs. (17) and (18), one observes that $T2 < T1$. Hence, a 128-point FFT can be used to compute the range correlation for the real-time low-resolution image mode for $\theta = 25^\circ$.

Case 2: For $\theta = 52^\circ$, using the same procedure as in Case 1, one can show that $n = 256$ points, $T1 = 4.6 \times 10^{-4}$ sec and $T2 = 12.8$ μsec. Thus, $T2 < T1$. Hence, a 256-point FFT can be used to compute the range correlation for the real-time VOIR-SAR low-resolution image mode for $\theta = 52^\circ$.

IV. Implementation of the Azimuth Correlator

In order to compute the azimuth correlation, one needs to compute the number k_a of points of the reference filter per look, for the low-resolution imaging mode. The number of points of the reference filter per look is given by

$$k_a = \tau_a \times PRF \tag{19}$$

The total number of points of the reference filter for all looks is given by

$$k = Nk_a \tag{20}$$

From the parameters given in Table 1, one can compute k_a and k for the low-resolution imaging modes as follows:

Case 1: $\theta = 25^\circ$. From Eqs. (1a) and (1b),

$$R = \frac{300 \text{ km}}{\cos 25^\circ} = \frac{300 \text{ km}}{0.906} = 331.13 \text{ km}$$

$$L_a = \frac{\lambda R}{2\Delta Z} = \frac{0.235 \times 331.13 \times 10^3}{2 \times 300} = 129.7 \text{ m}$$

$$\tau_a = \frac{L_a}{v} = \frac{129.7}{6.6 \times 10^3} \cong 0.019 \text{ sec}$$

$$k_a = \tau_a \times PRF = 0.019 \times 2180 = 41.42 \text{ points} \quad (21a)$$

$$k = N \times k_a = 24 \times 41.42 \cong 994 \text{ points} \quad (21b)$$

Case 2: $\theta = 52^\circ$, from Eqs. (1a) and (1b)

$$k_a = 0.029 \times 2180 = 63 \text{ points} \quad (22a)$$

$$k = 24 \times 63 = 1517 \text{ points} \quad (22b)$$

To use the FFT for implementing the azimuth correlator, let

M_i $(1 \leqslant i \leqslant 3)$: memory to store the range lines for azimuth processing; capacity of each M_i for $i = 1, 2, 3$ is $k_a \times r$ complex data, or $k_a \times r$ bytes.

A_i $(1 \leqslant i \leqslant N)$: memory to store the output of azimuth correlator; capacity of each A_i is $(k_a/N) \times r$ real data or $(k_a/N)(r/2)$ bytes.

$T3$: time required to store k_a range lines into M_1 or M_2 or M_3.

$T4$: total computation time of the azimuth correlation of the $2k_a$ range lines and the k_a range filter of all looks.

The overlap-add FFT for computing multiple looks azimuth correlator is suggested by Wu (Ref. 6). For more detail see (Ref. 2). A detailed design of an azimuth correlator for the low-resolution imaging mode is given in Fig. 2. Figure 2 shows that a combination of the overlap-add FFT and pipeline technique can be used to implement the azimuth correlator for the real-time VOIR-SAR low-resolution imaging mode. To illustrate the processing described in Fig. 2, consider three looks for the reference filter, i.e., $N = 3$. The processing is composed of the following steps.

Step 1: The $2k_a$ range lines of complex data in M_3 and M_1 is passed to the azimuth correlator while the M_2 is being stored with k_a range lines of complex data. In the azimuth correlator, $2k_a$ range lines of input data are now convolved with the first look of k_a range lines of the reference filter. This can be performed by using an n-point FFT, where $n \geqslant 2k_a$. After performing the convolution of the third look, only k_a/N lines of real data (each line has r points) becomes output and is added into A_1 in the overlap-add processor. The processing is repeated for the second look of the reference filter while the k_a/N image lines in A_1 are being read out. When the azimuth correlation is accomplished for the second look, the k_a/N output lines of real-data for the second look is added to A_2 in the overlap-add processor, while A_1 is set to zero. Finally, the processing is repeated for the first look reference filter. When the processing is accomplished, the k_a/N output lines of real data for the first look is added into A_3 in the overlap-add processor. It should be emphasized that timing considerations require all azimuth processing described in this step be completed before the k_a range lines are loaded into M_2, i.e., $T4 < T3$.

Step 2: When all k_a range lines are loaded into M_2, the $2k_a$ range lines of complex data in M_1 and M_2 are passed to the azimuth correlator while M_3 is being filled with the next k_a range lines. Using the same procedure as the azimuth correlator in Step 1, the $2k_a$ of range lines are correlated with the third, the second, and the first look sequentially. The k_a/N lines output of the third look is added to A_2. Then the k_a/N lines output of the second look is added to A_3 while the k_a/N image lines in A_2 are being read out. Finally, the k_a/N line output of the first look is added to A_1, while A_2 is set to zero.

Step 3: When all k_a range lines are loaded into M_3, the $2k_a$ range lines of complex data in M_2 and M_3 are passed to the azimuth correlator while M_1 is being filled with the next k_a range lines. Using the same procedure for azimuth correlation as in Step 1, the $2k_a$ of range lines are correlated with all looks of the reference filter sequentially. The k_a/N lines output of the third look is added to A_3. Then the k_a/N lines output of the second look is added to A_1 while the k_a/N image lines in A_3 are read out. Finally, the k_a/N lines output of the first look is added to A_2, while A_3 is set to zero. The processing is repeated for Step 1.

From the above procedure, one observes that if $T4 < T3$, then the FFT can be used to compute one-dimensional azimuth correlation for the real-time VOIR-SAR low-resolution imaging mode. To show this, one needs to compute the $T3$ and $T4$ as follows:

In order to use the FFT to correlate the k_a-point azimuth filter with $2k_a$ input data, one needs to choose n such that $n \geqslant 2k_a$, where n is a power of 2. To do this, we first take the n-point transform of input data, then multiply the transform of the input data by the transform of filter function. It can be shown that the transforms of the filter function have approximately 8 nonzero values for $\theta = 25$ and $\theta = 52$. Thus, the number of points in the product of the transform of input data and of the filter is 8. Since the k_a/N-point output of the correlation of the k_a-point filter and $2k_a$-point input data is needed to add into A_i, where $1 \leqslant i \leqslant N$, then each row of each of the N looks requires $15 \times k_a/N$ complex additions and

$16 \times k_a/N$ complex multiplications to accomplish the inverse transformation and complete the correlation. It follows from a current TRW multiplier specification sheet that the time required to compute either a 16-bit addition or multiplication should be between 100×10^{-9} and 200×10^{-9} sec. If one uses a parallel pipeline technique to compute the inverse transform, then $T4$ is

$$T4 \cong r \times \tau_n + N \times r \times 4 \times 200 \times 10^{-9} \qquad (23)$$

The time required to store the k_a range lines into M_1 or M_2 or M_3 is

$$T3 = k_a \times T1 \qquad (24)$$

where $T1$ is the computation time required to load m range data points into a buffer, as computed in Eq. (15).

Case 1: For $\theta = 25°$, from Eq. (13)

$$r = n - \ell + 1 = 108 - 26 + 1 = 83 \text{ points}$$

From Eq. (21a) we know $k_a = 41 \cong 48$. Thus

$$M_i = k_a \times r = 48 \times 83 = 3984 \text{ bytes for } 1 \leqslant i \leqslant 3.$$

Since $N = 24$, the $k_a/N = 48/24 = 2$ lines are output for each look. Thus,

$$A_i = k_a/N \times r/2 \cong 2 \times (83/2) \cong 83 \text{ bytes for } 1 \leqslant i \leqslant 24$$

From Eq. (24), it follows that

$$T3 = 48 \times 4.56 \times 10^{-4} = 218.88 \times 10^{-4} \text{ sec}$$

where $T1 = 4.56 \times 10^{-4}$ sec is given in Eq. (17). Since the time for computing a 128-point is 6.4 μsec, by Eq. (23)

$$T4 = 83 \times 6.4 \times 10^{-6} + 24 \times 83 \times 0.8 \times 10^{-6}$$

$$\cong 21.25 \times 10^{-4} \text{ sec}$$

Case 2: For $\theta = 52°$, from Eq. (14),

$$r = n - \ell + 1 = 252 - 26 + 1 = 227 \text{ points}$$

From Eq. (22a)

$$k_a = 63 \cong 72$$

Thus

$$M_i = k_a \times r = 72 \times 227 = 16344 \text{ bytes for } 1 \leqslant i \leqslant 3$$

Since $N = 24$, then $k_a/N = 72/24 = 3$ lines is output for each look. Thus

$$A_i = 3 \times 227/2 \simeq 340 \text{ bytes for } 1 \leqslant i \leqslant 24$$

From Eq. (24), it follows that

$$T3 = 72 \times 4.6 \times 10^{-4} \cong 331.2 \times 10^{-4} \text{ sec}$$

where $T1$ is 4.6×10^{-4} for $\theta = 52°$ in Section III.

From Eq. (23),

$$T4 = 6.4 \times 10^{-6} \times 227 + 24 \times 227 \times 0.8 \times 10^{-6}$$

$$\cong 58.11 \times 10^{-4} \text{ sec}$$

In Case 1 and Case 2, one observes that $T4 < T3$. Hence a 128-point FFT can be used to compute the azimuth correlator for the real-time VOIR-SAR low resolution image mode for $\theta = 25°$ and $\theta = 52°$.

Acknowledgment

The authors express thanks to Dr. C. Wu for his many helpful suggestions on the subject of SAR.

References

1. "VOIR-SAR System Design – 1978," Interim Report, Jet Propulsion Laboratory, 1978.
2. W. J. Van de Lindt, "Digital Technique for Generating Synthetic Aperture Radar Images," IBM J. Res. Develop., September 1977.
3. C. Wu, C. F. Leang, B. Barkan, and S. Pang, "An Introduction to the Interim Digital SAR Processor and the Characteristics of the Associated Seasat SAR Imagery," Interim Report, Jet Propulsion Laboratory, Pasadena, California, 1979.
4. K. Tomiyasu, "Tutorial Review of Synthetic-Aperture Radar (SAR) With Applications to Imaging of the Ocean Surface," Proceedings of the IEEE, Vol. 66, No. 5, May 1978.
5. E. O. Brigham, *The Fast Fourier Transform*, Prentice-Hall, Inc., Inglewood Cliffs, New Jersey, 1974.
6. C. Wu, "A Digital System to Produce Imagery From SAR," AIAA Systems Design Driven by Sensors, Pasadena, California, October 18-20, 1976.

Table 1. VOIR-SAR system characteristics

Altitude:	300 ± 25 km			
Frequency:	1275 MHz			
Antenna:	2.7 × 7.0 m planar array			
Minimum radar cross section:	−30 dB at 0 dB SNR (over swath)			
Peak output power:	100 W			
Spacecraft speed:	6.6 km/s			
	Low resolution		High resolution	
	Incident angle		Incident angle	
	25°	52°	25°	52°
Average power (W):	6		15	
Bandwidth (MHz):	0.8		4.75	
Pulse length (μsec):	28		47.5	
System ISLR (dB):	−13.6		−11.0	
Quantization bits:	5		3	
Maximum data rate (Mbps):	3.20		7.20	
Number of looks:	24		8	
Resolution (range & az):				
Line pair (m):	600/600	1150/600	100/100	200/100
Radar (m):	300/300	575/300	50/50	100/50
Pixel (m):	180/180	345/180	30/30	60/30
Swath width (km):	50	40	12	12
Dynamic range (dB):	30	37	17	21
Noise eq. σ_0 (best) (dB):	−37	−45	−32	−39
PRFs (Hz):	5 from 1923 to 2180		5 from 2835 to 3165	

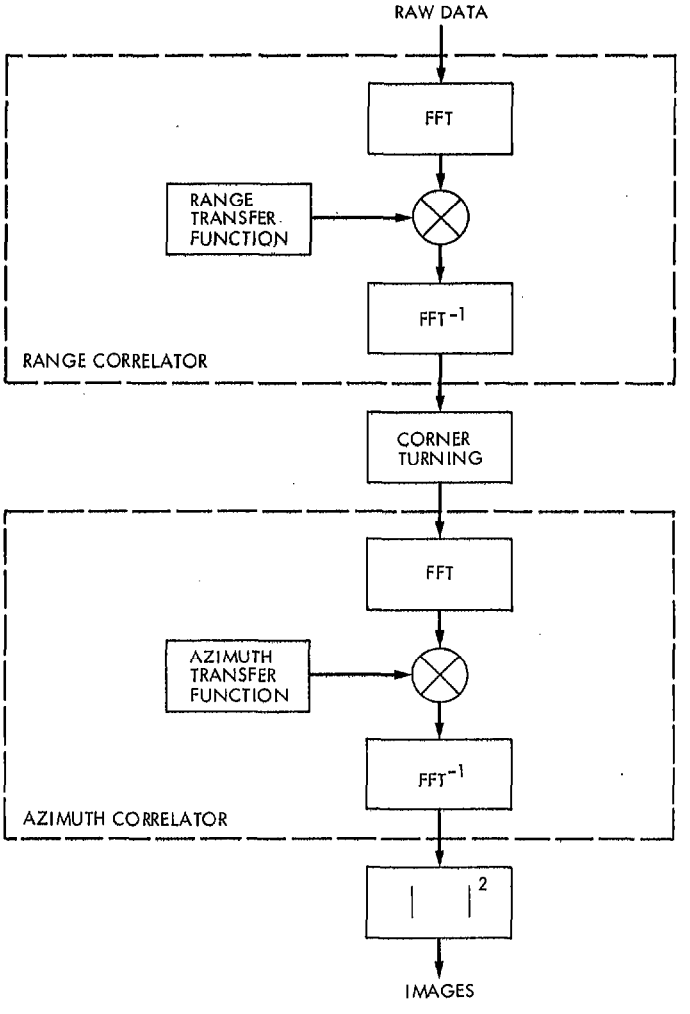

Fig. 1. A block diagram of the FFT-SAR data processing

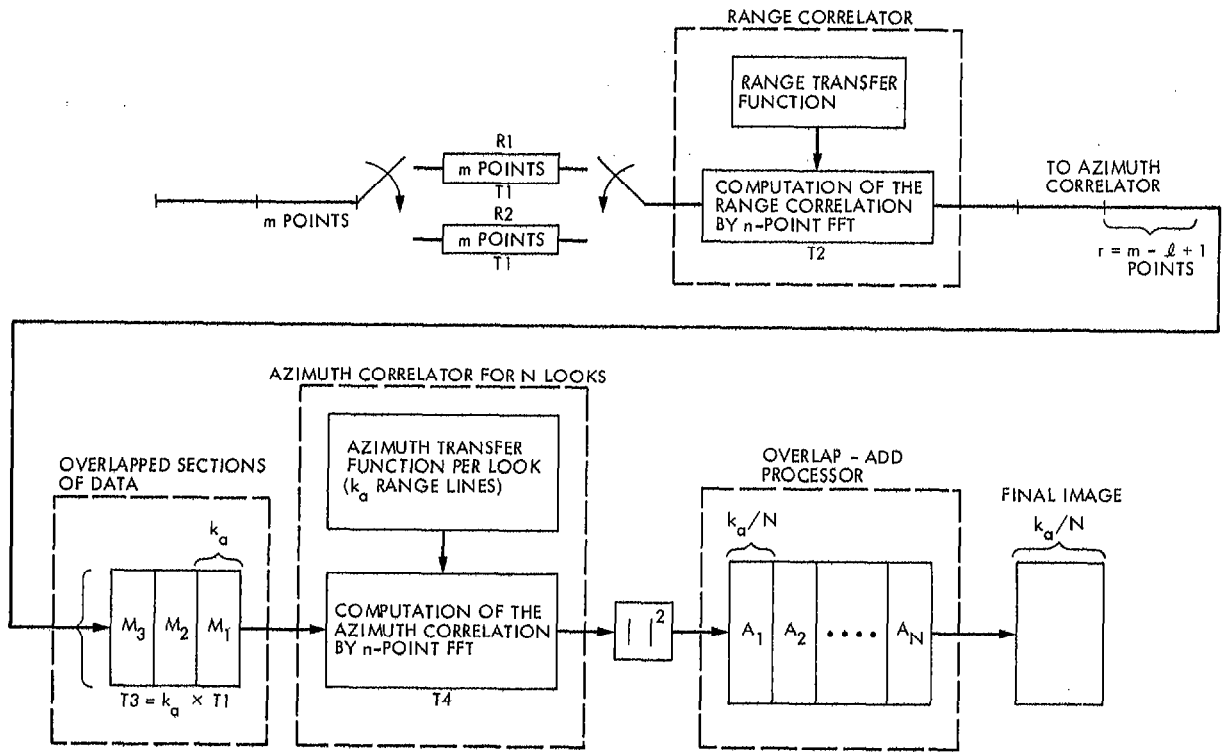

Fig. 2. A flowchart of the range and the azimuth correlator for the real-time low-resolution SAR-VOIR imaging mode by using an FFT method